IEEE Access
Multidisciplinary ⋮ Rapid Review ⋮ Open Access Journal

Received February 7, 2021, accepted February 20, 2021, date of publication March 4, 2021, date of current version March 18, 2021.

*Digital Object Identifier 10.1109/ACCESS.2021.3063810*

# Design and Performance Analysis of Tandem Organic Solar Cells: Effect of Cell Parameter

**FARHA ISLAM MIME[1], MD. RAFIQUL ISLAM[1], (Member, IEEE), EKLAS HOSSAIN[2], (Senior Member, IEEE), IBRAHIM M. MEHEDI[3,4], AND MD. TANVIR HASAN[5], (Member, IEEE)**

[1]Department of Electrical and Electronic Engineering, Khulna University of Engineering and Technology (KUET), Khulna 9203, Bangladesh
[2]Department of Electrical Engineering and Renewable Energy, Oregon Institute of Technology, Klamath Falls, OR 97601, USA
[3]Department of Electrical and Computer Engineering (ECE), King Abdulaziz University, Jeddah 21589, Saudi Arabia
[4]Center of Excellence in Intelligent Engineering Systems (CEIES), King Abdulaziz University, Jeddah 21589, Saudi Arabia
[5]Department of Electrical and Electronic Engineering, Jashore University of Science and Technology (JUST), Jashore 7408, Bangladesh

Corresponding author: Md. Tanvir Hasan (tan_vir_bd@yahoo.com)

**ABSTRACT** An organic solar cell (OSC), competitive with traditional one (Si-based), draws attention to future renewable energy sources due to its low-cost and continually rising efficiency. The tandem or multijunction structure undoubtedly offers an efficient way to boost the performance of OSCs. This work has explored the optical modeling of different organic photoactive materials to identify the potential materials for efficient tandem structure. The performance of double, triple, and quadruple junction tandem OSCs with suitable bandgaps has been analyzed with photoactive materials. The absorption efficiency enhances considerably using the thickness optimization of each subcell in tandem structures. Current matching in all subcells, an essential factor for efficient device operation, is taken into account while optimizing tandem structures. The quadruple design can achieve better photovoltaic performance than double or triple junction devices. The efficiency predicted from our proposed quadruple structure is ∼15.45%, with a short-circuit current density, $J_{SC}$ of ∼9 mA/cm$^2$ and an open-circuit voltage, $V_{OC}$ of ∼2.64 V. These results are one of the high-performance in terms of organic photovoltaic (OPV). Therefore, the above findings indicate that OSCs are very potential for future photovoltaic applications.

**INDEX TERMS** Tandem organic solar cells (OSCs), quadruple-junction, optical modeling, thickness optimization, current matching.

## I. INTRODUCTION

Photovoltaic (PV) industry is currently led by inorganic crystalline Si-based photovoltaics (PV), which are too expensive and mostly reliant on government financial assistance. This situation clarifies why PV only considers for a partial contribution to the world's electricity production. The possibility of additional cost reduction enhances the recognition of thin-film solar cells. Even with their lower efficiencies, thin-film solar cells make significant market penetration because of tradeoffs between efficiency and cost. An organic solar cell (OSC) absorbs light and transports charge by conductive organic materials for producing electricity from sunlight using the photovoltaic effect. The OSCs are solution-processed and can be printed or coated instead of using expensive vacuum deposition. The feasibility of low-cost production has yielded organic photovoltaic (OPV) technologies that pay more attention [1]. The first certified OSC has been reported with an efficiency above 10% [2], which definitely opens a new era for its commercialization. During the last decade improvements in the performance of OSCs have been remarkable. The power conversion efficiency (PCE) has been enhanced from ∼5% to a recent value of ∼14% [3], [4]. High-quality OSCs are now routinely developed, which reflected in the reported internal quantum efficiency (IQE) and fill-factor (FF) as ∼90% and ∼70%, respectively [5]. All these traits added to open the way to commercialize the OPV technology. However, single-junction OSCs suffer from a short absorption range, limiting the use of full solar spectrum [6], and low-carrier mobility, which results in a low-photocurrent to produce low-PCE [7]. Researchers are doing continuous efforts to defeat the present shortcomings of OSCs. The low-charge carrier mobilities of OPV limit an active layer's thickness to several hundred nanometers, which

The associate editor coordinating the review of this manuscript and approving it for publication was Giovanni Angiulli.

allows the free charge carriers to shift to their corresponding electrodes before recombination. The photoactive layer thickness is usually adjusted, in the range of ∼50 to 300 nm depending on the semiconductors' actual nature, to find the optimum performance. Organic materials have a relatively high-absorption coefficient ($\sim 10^5$ $cm^{-1}$), which partially settles the low-mobility issue. Though the mobility has been controlled to some extent, the absorption efficiency is considerably improved using tandem configurations. In tandem cell configurations, two or more subcells have their corresponding absorption spectra, assembled in a single structure, and tied in series or parallel offer enriched photon absorption and consequently lifted the PCE [8]. The light that the high bandgap bottom device cannot absorb can further intrude on the low bandgap's top cell. The wide bandgap material has a usually higher voltage, lower photocurrent, and smaller bandgap material has higher photocurrent and lower voltage. The tandem structure offers maximization of the open-circuit voltage by reducing thermalization losses as compared to that of a single-junction having low-bandgap [2]. Different groups are carrying out considerable research efforts both experimentally and theoretically to improve the device performance of OSC. Theoretical optimization is helpful as it gives an important insight into a device. Arnab *et al.* reported an analytical model for photocurrent, which depends on voltage, considering exponential photon absorption [9]. Later, the same research group modified their model by solving continuity equations for charge carriers with proper boundary conditions and Shockley-Read-Hall (SRH) recombination [10]. They have considered exponential photon absorption considering Beer-Lambert law in both models. The assumption of exponential photon absorption is not appropriate for OSCs as these devices' layer thickness is very tenuous. The optical interference-effect significantly influences light absorption. For organic material, the effect of interference cannot be overlooked [11] and influences the final efficiency. To capture these features, a better method for calculating the intensity of light distribution within the active layer is the Transfer Matrix Method (TMM). Earlier, TMM was developed to analyze the propagation of electromagnetic waves in stratified media, and later, it has been employed to analyze the optical electric field distribution inside thin-film solar cells [12].

Generally, after the photon absorption, created excitons diffused to the donor-acceptor (D-A) interface and dissociated. The excitons are either suffer geminate type recombination or able to be separated into free carriers. Researchers assume that all excitons dissociated into free charge carriers [13]–[16], whereas some of them [9], [10], [17] mentioned that the final photocurrent of OSC is controlled by the dissociation efficiency of bound electron-hole pair (EHP). Some models calculate OPVs' dissociation efficiency using the Onsager model [18] while some others use the modified Braun model in their works [9]–[11]. Onsager-Braun approximation assumes the presence of a long-range electric field located inside the active layer. However, this field's presence is still under debate and some researchers claim a complete diffusion-driven charge transport inside the OPV device [19]. The dissociation efficiency is reported near to unity for PCDTBT:PCBM material [20]. The exciton dissociation rate equal to unity means the exciton generation rate only depends on the number of photons absorbed in the active layer [13]. Again, after dissociation, free charge carriers may recombine while traveling towards the electrodes [21]. It is claimed that once an exciton dissociated into free carriers, their collection efficiency is very high (∼100%) at the opposing electrodes [22]. Many theoretical works ignore the charge carriers' recombination due to simplicity without significant deviation from experimental results [14], [23]. Therefore, photons' absorption inside the active layer gives important prediction of the final device current in OSCs. Still, many researchers have been looking for different mixtures of organic material to achieve high-efficient tandem OSCs. The first quadruple junction OSC is reported by Rasi *et al.* [24]. They reported that their modeled subcells showed sufficient current mismatch, where the back cell was limiting the current. However, in most works on tandem organic solar cells, the current matching is largely discarded. Therefore, the optimization of current generated by each cell subcell is essential for avoiding extra charges and the local electric field, which eventually reduces efficiency [25]. Also, optimizing individual subcells' layer thickness is required to maximize short-circuit current density and current matching of multijunction cells.

The summary of the contributions of this article is presented below:

1) The critical challenge in designing the triple and quadruple junction OSC is that the existing organic photoactive layer having absorption greater than 1200 nm has not been reported yet. A higher photocurrent is expected from low bandgap photosensitive polymer through the harvesting of energy further into the infrared region. Tandem structures offer increased spectral coverage; thus, more photons with different ranges of energies are absorbed. When stacking multiple absorbers in tandem structures, the high bandgap material is placed near the anode. The light enters the device to absorb the photon with high energy, leaving low energy photons for the next absorbers to harvest. In our work, we have designed and optimized the tandem OSCs with the quadruple junction. To choose the organic materials and thickness of the structure, we have systematically estimated the performance for single-junction to quadruple junction OSCs. The tandem structures' subcells are considered as series-connected. In series-connected tandem cells, the total short-circuit current density is equal to the minimum current of the subcells, whereas the total open-circuit voltages are the sum of each subcell's junction voltages [8].
2) The performance of different organic active layers in their single-junction architectures have been studied.

It is noted that different research groups produce many organic materials yielding high efficiencies in minimal amounts that considerably limit their access and reproducibility. Therefore, while choosing materials for our theoretical calculation, commercially available and the materials used by many research groups are chosen to overcome the aforementioned problems. Again, these increase the achievability and reliability of our proposed structures. The optical optimization has been carried out in this work concerning various cell parameters that play a crucial part in the OPV's performance exploration. The optical spacer layer's effect in the electron-hole pair (EHP) generation is quantified.

3) The main focus is to propose an efficient quadruple structure with better achievable efficiency. Limited tandem cell current is mainly due to spectral overlapping and current mismatch of subcells. As in tandem structure, the lowest current supplied by any of the subcells will be the final device current; careful selection of materials and fine-tuning of current density is required to obtain efficient performance. Optimization of individual subcells' layer thickness is needed to maximize current density and current matching of multijunction cells. In this study, optimization of current density for the tandem cell is performed with proper consideration of different subcells' current matching.
4) There is still no work on the interdependence of subcells for quadruple structures to the best of our knowledge. Therefore, changing one layer's thickness affects other subcells in tandem structures that have been explored in the proposed quadruple OSC. We also consider parasitic absorption and transmission losses. As different cell parameters are studied carefully, overestimations of efficiencies are expected to be avoided. Finally, we show that tandem OSC's efficiency increases in quadruple-junction than double- and triple- junction configurations.

The remainder of the paper is organized as follows:

Section II describes the theoretical design of proposed tandem OSCs with the properties of the organic materials and the considered model of this work. The performance of OSCs have been analyzed for different cell parameters in section III. Finally, Section IV summarizes this work.

## II. DEVICE DESIGN AND COMPUTATIONAL METHODOLOGY

We have designed and optimized a quadruple junction OSC to attain a high PCE. **Figure 1** illustrates the proposed OSC with a quadruple structure. The device structure is comprised of 13 functional layers, among which four are organic photoactive materials. Different organic materials with various optical bandgaps are studied as the active layers to achieve an efficient tandem structure. Firstly, the front subcell consists of donor material, poly [N-900-heptadecanyl-2,7-carbazole-alt-5, 5-(40,70-di-2-thienyl-20,10,30 benzothiadiazole)] (PCDTBT), which combine with PCBM

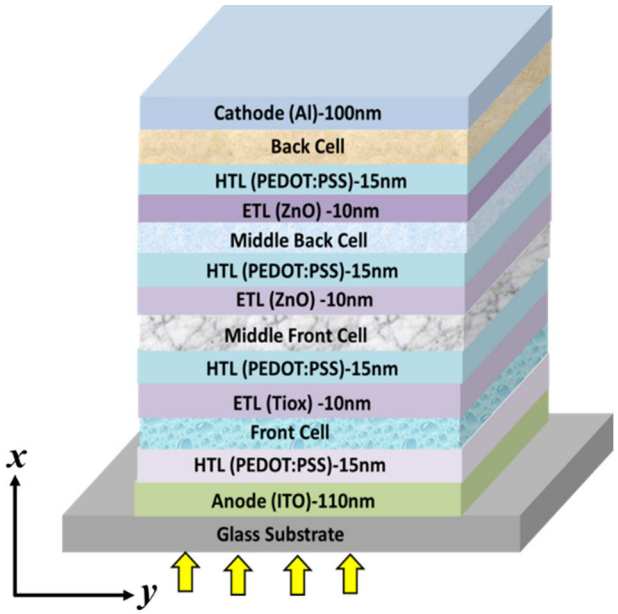


**FIGURE 1.** Schematic device architecture of quadruple-junction OSC.

as acceptor material. This material combination is very suitable for attending enhanced open-circuit voltage as ∼0.9 V because of the highest occupied molecular orbital (HOMO) is located at 5.5 eV [26]. Secondly, there are three different materials are considered to optimize the middle front subcell. These donor materials are poly[[4,8-bis[(2-ethylhexyl)-oxy]benzo[1,2-b:4,5-b0]dithiophene-2,6-diyl][3-fluoro-2-[(2-ethylhexyl)carbonyl] thieno[3,4-b] thio ph-enediyl]] (PTB7) [27], poly[(ethylhexyl-thiophenyl)-benzo-dithiophene- (ethylhexyl)-thienothiophene] (PBDTT T-EFT, usually defined as PTB7-Th or PCE10) [28], and poly[3,6-bis-(40-dodecyl-[2,20] bithiophenyl-5-yl)-2, 5-bis-(2-ethyl-hexyl) -2,5 dihydropyrrolo [3], [4] pyrrole-1, 4-dione] (pBBTDPP2) [29] which are combined with the acceptor PCBM. The PTB7-Th has red shifted absorption spectra having a bandgap of 1.58 eV which is smaller than PTB7 material (1.64 eV) and allows more photons to absorb for enhancing charge generation [30]. The low bandgap pBBTDPP2 (1.4 eV) covers the absorption spectrum up to 900 nm. Thirdly, the middle back subcell consists of poly[[2,5-bis(2-hexyldecyl-2,3,5,6-tetrahydro-3,6 dioxopyrrolo[3,4-c] pyrrole-1,4-diyl]-alt-[3′,3″-dimethyl 2,2′ : 5′, 2″-terthiophene] -5,5″-diyl] (PMDPP3T) (1.3 eV), which exhibits solar spectra coverage of ∼1000 nm [31]. Finally, the poly[[4-(2-ethylhexyl)-4Hdithieno [3,2-b:2′,3′-d] pyrrole-2,6-diyl]-alt-2,5-selenophenediyl[2,5-bis (2 ethylhexyl)-2,3,5,6-tetrahydro-3,6-dioxopyrrolo[3,4-c]-pyrr-ole-1, 4-diyl]-2,5-selenophenediyl] (PDPPSDTPS) (1.13 eV) is considered as the back subcell [32]. This donor material has the longest absorption range than other materials having spectral fill up to 1200 nm when mixed with acceptor PCBM. **Figure 2 (a) and (b)** show the refractive indices of the concerned organic materials considered directly from the

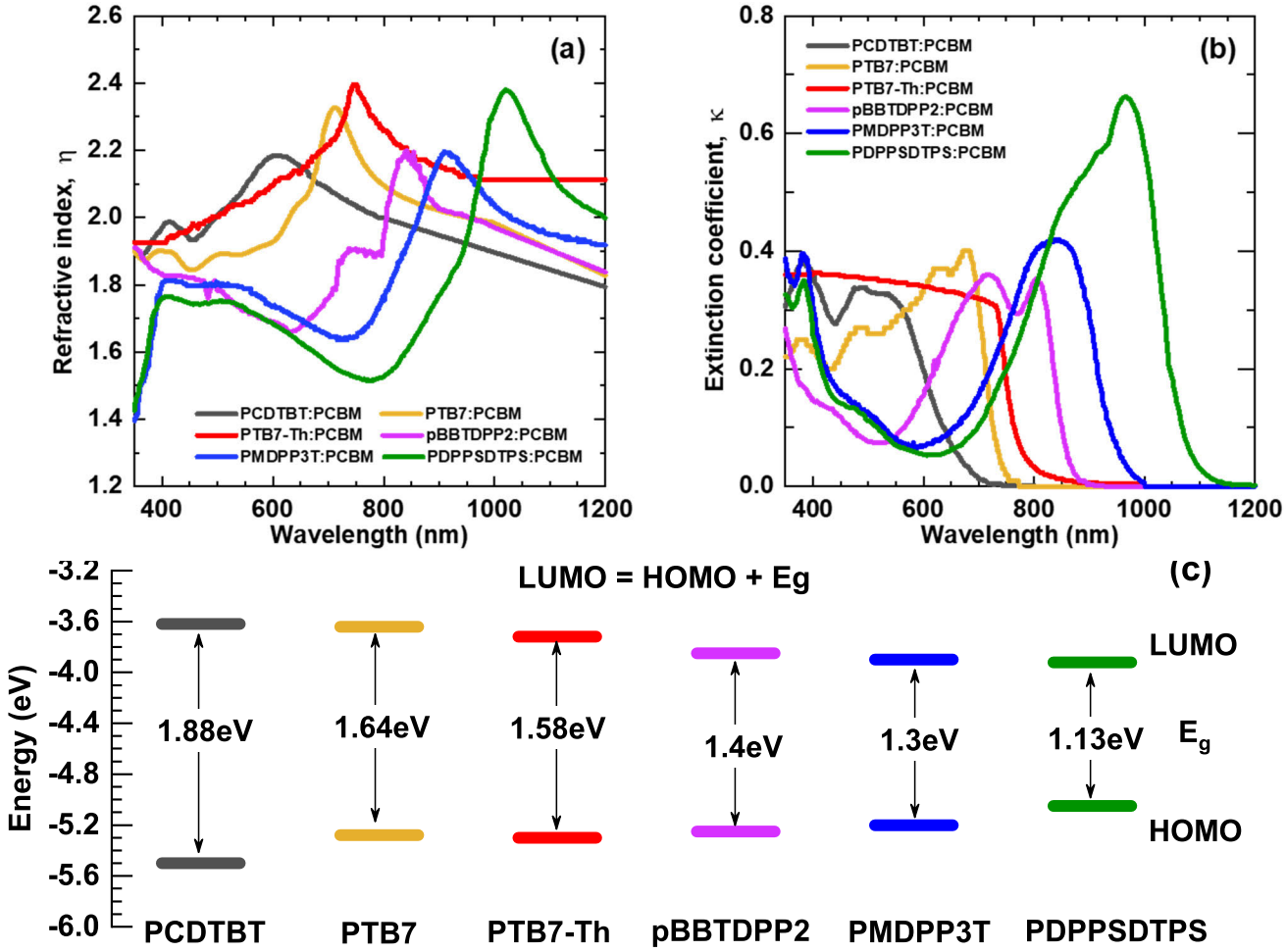


**FIGURE 2.** Refractive index, $\eta$ (a) and Extinction coefficient, $\kappa$ (b) values of different organic materials employed in the active layers (c) energy level diagram of considered organic materials.

reported data [24], [30], [33]–[35]. The bandgap of these materials varies from 1.9eV $\sim$ 1.13eV. We have considered the materials' bandgap and HOMO level from the reported data [26], [29]–[32], [36]. The LUMO level is determined from the HOMO and optical bandgap as LUMO = HOMO + $E_g$. **Figure 2(c)** represents the bandgap of considered donor material along with HOMO-LUMO levels. Here, $TiO_x$ and ZnO are considered as the electron transport layer (ETL) while the hole transport layer (HTL) is poly (ethylenedioxythiophene):poly (styrenesul-fonate) (PEDOT: PSS). The transparent ITO acts as anode whereas the cathode is made of Aluminum (Al).

Usually, Beer-Lambert (BL) law is considered to estimate the light intensity inside the device. The light intensity decay exponentially with distance as $I(x) = I_0 \exp(-\alpha x)$ where $I(x)$ is the intensity of light at position $x$, $I_0$ is the incident light intensity, $\alpha$ is the absorption coefficient. In OPV, the active layers' typical thickness is confined in the range of 20 to 300 nm [37]. The BL exponential decay of light intensity is not straightforward behavior inside the OSC. To evaluate the optical process, it is essential to include both transmission of electromagnetic waves inside the device and reflectance from layers as well as electrodes. Successive transmissions and reflections generate optical interference in the material stack. In thin OSCs, the effect of interference due to forward and backward directed light cannot be neglected to evaluate the performance. This phenomenon inside the OSCs is considered by optical Transfer matrix method (TMM). Optical TMM assumes light as a plane wave. The constituent materials are considered to be homogeneous and isotropic so that their optical response can be described by complex index of refraction, $\tilde{\eta_J} = \eta_j + ik_j$, where $\eta_j$ is the refractive index and $k_j$ is the extinction coefficient [12]. Both $\eta_j$ and $k_j$ are the function of wavelength of incident light. The interfaces are assumed to be optically flat. With these assumptions, the propagation of light can be described by a $2 \times 2$ matrix. This method takes into accounts the layers' thicknesses; refractive index and extinction coefficient of all the materials that constitute a device is implemented by McGehee group [38]. Therefore, the effect of any change in any layer thickness or change of optical properties can be determined by this method.

To evaluate the optical field induces from an incident plane wave on the photovoltaic active region, the multilayer structure of an OSC is considered to embed between two semi-infinite layers ($j = 0, j = m + 1$). The light is assumed to incident from the left on a multilayer device having $m$ layers surrounded by ambient (air) and a substrate at two sides. Each layer $j$ ($j = 1, 2, \ldots, m$) of the multilayer structure has a corresponding thickness $d_j$. The primary process to produce the photocurrent in an OSC is the generation of bound EHP called excitons due to absorbing photon energy from optical electric field. For interference, the optical electric field at any point $x$ has two components: one component propagating in the positive $x$ direction $E_j^+(x)$ and another in the negative $x$ direction $E_j^-(x)$. This interference affects the optical electric field density across the device and, consequently, absorbs light in the active layer. The optical electric field at a distance $x$ within layer $j$ can be expressed as [11]:

$$E_j(x) = E_j^+(x) + E_j^-(x). \tag{1}$$

When sunlight passes from one layer to adjacent layer in a multilayer structure, light is reflected and refracted. The behavior of incident light between two adjacent layers (e.g., layer $j$ and layer $k$) is described by the interface matrix $I_{jk}$. The interface matrix can be expressed as [11]:

$$I_{jk} = \begin{bmatrix} (\tilde{\eta_J} + \tilde{\eta_k})/2\tilde{\eta_J} & (\tilde{\eta_J} - \tilde{\eta_k})/2\tilde{\eta_J} \\ (\tilde{\eta_J} - \tilde{\eta_k})/2\tilde{\eta_J} & (\tilde{\eta_J} + \tilde{\eta_k})/2\tilde{\eta_J} \end{bmatrix} \tag{2}$$

where $\tilde{\eta_J}$ and $\tilde{\eta_k}$ are the complex refractive indexes of layer $j$ and layer $k$. Again, when light propagates through a layer, light is absorbed, which represents as layer matrix $L_j$ and expresses by [11]:

$$L_j = \begin{bmatrix} \exp\left(-i\frac{2\pi\tilde{\eta_J}}{\lambda}.d_j\right) & 0 \\ 0 & \exp\left(i\frac{2\pi\tilde{\eta_J}}{\lambda}.d_j\right) \end{bmatrix} = \begin{bmatrix} \exp(-i\xi_j d_j) & 0 \\ 0 & \exp(i\xi_j d_j) \end{bmatrix} \tag{3}$$

where, $\xi_j = \frac{2\pi\tilde{\eta_J}}{\lambda}$ and $d_j$ is the thickness of layer $j$. By using interface matrix $I_{jk}$ and layer matrix $L_j$ the total system transfer matrix or scattering matrix $S$. The transfer matrix $S$ is the product of all interface and layer matrices as [12]:

$$S = \begin{bmatrix} S_{11} & S_{12} \\ S_{21} & S_{22} \end{bmatrix} = \left(\prod_{n=1}^{m} (I_{(n-1)n} L_n)\right) . I_{m(m+1)} \tag{4}$$

The total transfer matrix $S$ relates the optical electric field of the two outermost layers ambient and substrate ($j = 0$ and $j = m+1$).

$$\begin{bmatrix} E_0^+ \\ E_0^- \end{bmatrix} = \begin{bmatrix} S_{11} & S_{12} \\ S_{21} & S_{22} \end{bmatrix} \begin{bmatrix} E_{m+1}^+ \\ E_{m+1}^- \end{bmatrix} \tag{5}$$

In order to calculate the internal electric field in layer $j$, the total layer system may be split into two subsystems $S_j'$ and $S_j''$ separated by layer $j$. The total transfer matrix (S) can be redefined as [12]:

$$S = S_j' L_j S_j'' \tag{6}$$

where the subsystems transfer matrices $S_j'$ and $S_j''$ may be expressed as [12]:

$$S_j' = \begin{bmatrix} S_{j11}' & S_{j12}' \\ S_{j21}' & S_{j22}' \end{bmatrix} = \left(\prod_{n=1}^{j-1} (I_{(n-1)n} L_n)\right) . I_{j(j-1)} \tag{7}$$

$$S_j'' = \begin{bmatrix} S_{j11}'' & S_{j12}'' \\ S_{j21}'' & S_{j22}'' \end{bmatrix} = \left(\prod_{n=j+1}^{m} (I_{(n-1)n} L_n)\right) . I_{m(m+1)} \tag{8}$$

The optical electric field at a distance $x$ within layer $j$ can be expressed as [12]:

$$E_j(x) = \frac{S_{j11}'' e^{-i\xi_j(d_j - x)} + S_{j21}'' e^{i\xi_j(d_j - x)}}{S_{j11}' S_{j11}'' e^{-i\xi_j d_j} + S_{j12}' S_{j21}'' e^{i\xi_j d_j}} E_0^+ \tag{9}$$

From the distributions of optical and electromagnetic fields, the excitons generation rate is evaluated. The energy dissipation Q as a function of position and wavelength is given by [12]:

$$Q(x) = \frac{1}{2} c\epsilon_o \alpha_j \eta_j \left|E_j(x)\right|^2 \tag{10}$$

where $c$ is the speed of light, $\epsilon_o$ is the permittivity of free space, $\alpha_j$ and $\eta_j$ are the absorption coefficient and refractive index of layer $j$, respectively. The exciton generation rate can be expressed as [13]:

$$G(x, \lambda) = Q(x, \lambda)\frac{\lambda}{hc} \tag{11}$$

Finally, the exciton generation rate as a function of position can be obtained by integrating $G(x, \lambda)$ over the visible spectrum [13]:

$$G(x) = \int_{\lambda_1}^{\lambda_2} G(x, \lambda) d\lambda \tag{12}$$

For active layer thickness $= t$, the current density $J_{sc}$ (mA/cm$^2$) under AM 1.5G illumination is represented by:

$$J_{sc} = q \int_0^t G(x)\, dx \tag{13}$$

where $q =$ electron charge.

This method considers all the layers in order during the construction of any OSC architecture and the effect of adding or removing any layer.

The TMM method assumes that one absorbed photon produces one exciton, divided into free charges and collected at the respective electrodes that represent 100% IQE. It has been supported by experimental work that the IQE of organic material can reach 100% [26]. The IQE is considered as 100% to solely exploring the effect of photoactive layer thickness on light harvesting. The optical simulation has been carried out in the MATLAB environment. All the calculations have been done at room temperature. The simulation is done considering standard AM 1.5G (100 mW/cm$^2$) illumination. The flow

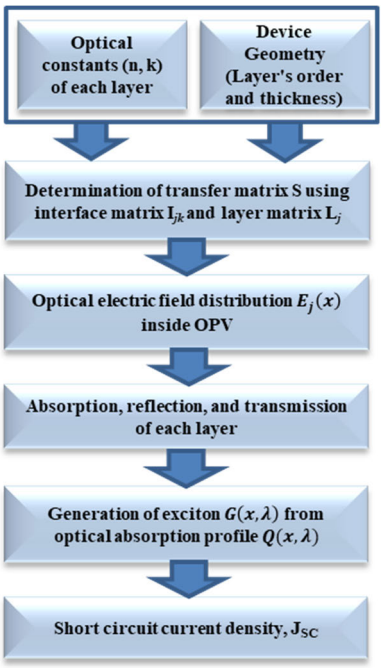


**FIGURE 3.** Flow diagram of the optical modeling through the transfer matrix method.

**TABLE 1.** Model validation by comparing with the experimental result.

| | $J_{SC}$ (mA/cm$^2$) | $V_{OC}$ (V) |
|---|---|---|
| Exp. [20] | -11 | 0.89 |
| Using our model | -11.62 | 0.90 |

diagram of the model is given in **Fig. 3**. In OSCs, the $V_{OC}$ generally depends on the difference between the HOMO level of donor material and the LUMO level of acceptor material and a deviation of ∼0.3 V is usually observed [39]–[41]. This deviation of 0.3 V is empirical, and it could be greater or lesser [41].

For validation test purposes, we have reproduced reported experimental results using our proposed simulation model.

The PCDTBT:PCBM based single-junction OSC with an active layer thickness of 150 nm is taken [20]. By considering the same device architecture and materials, a good match is found between the reported experimental data [20] and our simulated results using the proposed model, as shown in **Table 1**.

## III. RESULTS AND DISCUSSION

### A. SINGLE-JUNCTION OSC

The photovoltaic performance of six individual photoactive organic materials in their single junction structure has been investigated. The device architecture for single-junction is shown in **Fig 4 (a)**. The photoactive material is sandwiched between ITO, which acts as the anode, covered with PEDOT: PSS hole transport layer (HTL), and Al, which acts as the cathode. The thickness of all layers constituting the device architecture is kept fixed except the concerned active layers whose thickness varies from 0 to 300 nm. **Figure 4 (b)** shows the short-circuit current density as a function of the active layer thickness of the concerned materials. With the increase of thickness, a notable oscillation behavior is noticeably caused by optical interference between the incident light and the reflected light from the metal electrode. The commonly used active layer thickness in literature for the single-junction solar cells' performance study lies approximately 70 to 160 nm [42]–[46]. Therefore, we have chosen thickness within this range for the performance analysis of concerning organic materials in their single-junction structures where current density will have considerable value. **Figure 4(b)** shows that the effect of interference causes two position-dependent current density peaks for PCDTBT:PCBM material. Current density reaches its first peak for a layer thickness of around 70-90 nm. It is reported that the maximum efficiency for PCDTBT:PCBM material was obtained with the photoactive layer thickness in the range of 70-90 nm [47]. Again, the decrease in current density for larger thickness is observed following the second peak of current density for higher thickness. Similar experimental results were observed by Monestier *et al.* [13]. **Figure 4 (c) and (d)** show the short-circuit current density and the photon absorption profile at an optimized active layer thickness for the organic materials. In OSCs, maximum carrier generation may arise in inside of the active layer instead of at the edge due to various optical phenomena such as reflection and interference [12], [48]. These optical phenomena also provide numerous peaks in the distribution of the carrier generation rate [13]. **Figure 5** shows the exciton generation rate as a function of different active layer thickness for PCDTBT:PCBM material.

#### 1) EFFECT OF INTERLAYERS

Kim *et al.* [48] introduced an optical spacer layer between the active and metal electrodes to change the light intensity distribution inside the device spatially. The spatial rearrangement of optical electric field energy degeneracy (measured by $|E|^2$, where E is the optical electric field) causes the maximum light intensity to fall within the active layer for increasing the photon absorption [12], [48], [49]. **Figure 6** shows the optical electric field distribution of PCDTBT: PCBM material for a single wavelength of 545 nm. For thicker $TiO_x$, the electric field intensity inside the active layer is decreasing. Based on the active layer thickness, there lies optimum thickness for the optical spacer that enables to shift off the generation peaks [50]. The free carrier generation rate is related to the photogeneration of excitons, proportional to the optical electric field energy dissipation ($|E|^2$) [50]. Depending on the optical spacer layer's thickness, the effects on the generation of charge carriers and the maximum achievable current can be described. To analyze the device performances with optical spacer layers, two distinct single-junction structures are considered. The $TiO_x$ is employed between PCDTBT: PCBM and Al electrode. The ZnO is considered for PDPPSDTPS: PCBM structure.

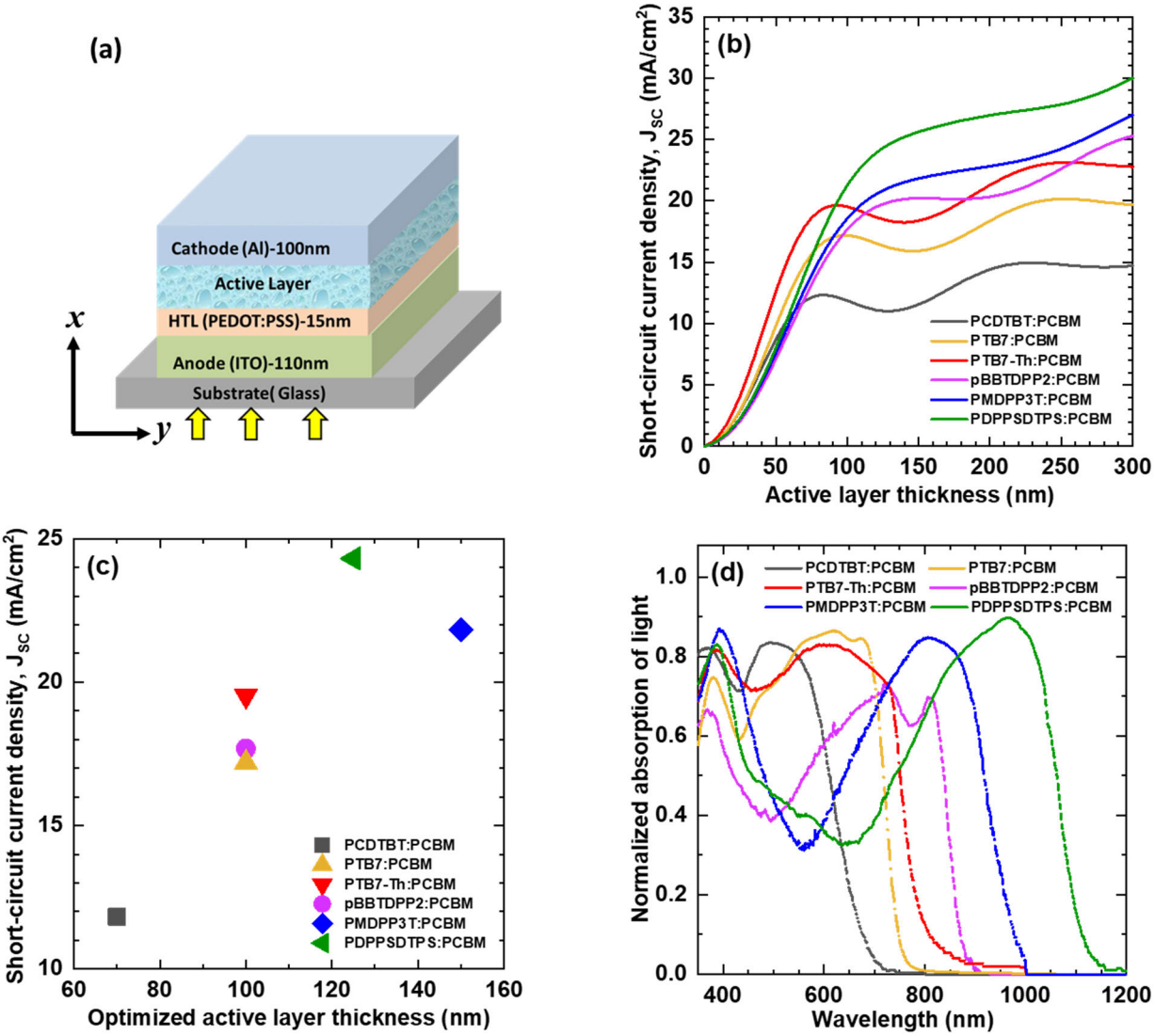


**FIGURE 4.** (a) Illustration of a single-junction OSC, (b) Effect of active layer thickness on short-circuit current density, $J_{SC}$ for different organic photoactive layers, (c) Optimize active layer thickness for respected organic materials, which are shown in (b), and (d) Normalized absorption of light which is estimated for optimized active layer thickness shown in (c).

**Figure 7** shows the short-circuit current density as a function of two optical spacer layer thicknesses, while the thicknesses of the active layers are remained fixed. For the blend thickness of 70 nm for PCDTBT: PCBM, the current density is found 11.83 mA/cm$^2$ while adding a thin layer of 10 nm $TiO_x$ increases the current to 12.07 mA/cm$^2$ without increasing the active layer thickness. These results indicate that the device current increased for a 10 nm layer of TiOx, whereas the current is decreased with the increase of TiOx more than 10 nm. Therefore, the optimum thickness of optical spacer layer TiOx is efficient at 10 nm for our concerned PCDTBT: PCBM material, which is in good agreement with previous reports [26]. The low bandgap material PDPPSDTPS: PCBM shows a very high current density of 24.31 mA/cm$^2$ at a layer thickness of 125 nm. Adding a ZnO layer between PDPPSDTPS:PCBM and Al, the device's performance might be enhanced. **In Fig. 7**, it is found that the optimum thickness for the optical spacer ZnO layer for this configuration is 20 nm. After reaching this optimum thickness, the overall current density decreased and degraded the device performance. Therefore, these results indicate that the device performance can be improved considerably using an optimum thickness of the interfacial layer without increasing the active layer thickness.

### *B. DOUBLE-JUNCTION OSC*

The PCDTBT: PCBM and PMDPP3T: PCBM having complementary absorption spectra can construct an efficient tandem structure from spectral coverage analysis. A double-junction tandem structure is considered PCDTBT: PCBM as front subcell and PMDPP3T: PCBM as back subcell, which are shown in **Fig. 8 (a)**. In a single-junction structure,

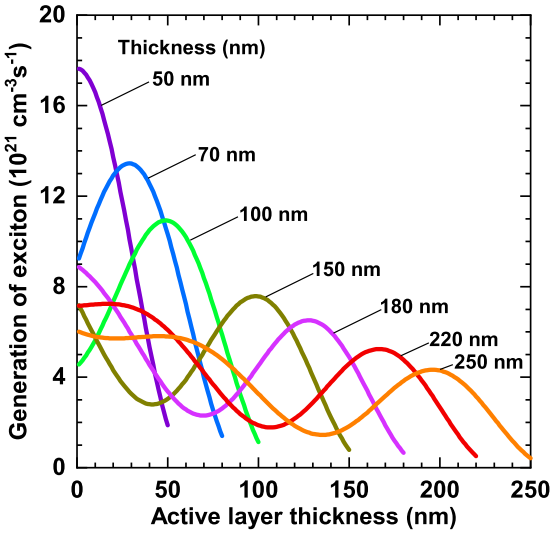


**FIGURE 5.** Exciton generation rate as a function active layer thickness for PCDTBT:PCBM material.

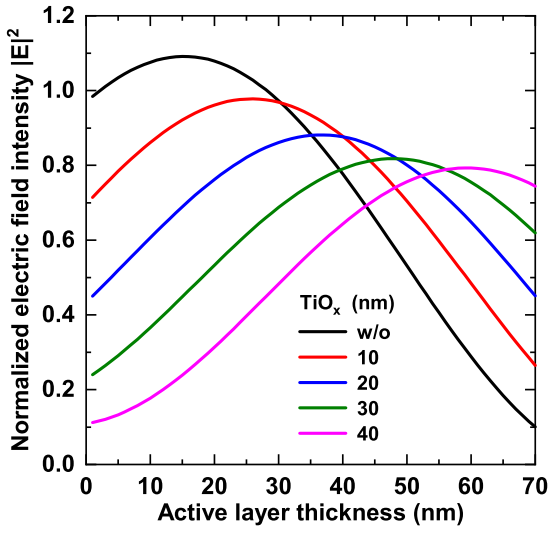


**FIGURE 6.** Normalized electric field intensity, $|E|^2$ of the active layer for various optical spacer layer, $TiO_x$ thicknesses.

the PCDTBT: PCBM material shows good absorption for the layer thickness of 70 nm while this material shows inferior absorption at that thickness in double-junction. This result indicates that photons' absorption by different materials performs differently from their single-junction structure to tandem structure. Optimization of layer thickness is essential for the performance analysis of multijunction cells. The efficiency of 8.90% in the tandem structure achieved by Li *et al.* for same materials where the layers thickness of 155 (front cell) and 150 nm (back cell) [31]. Using these thicknesses for the subcells in the proposed tandem cell shows a considerable enhancement in photon absorption, especially for PCDTBT: PCBM material, as shown in **Fig. 8 (b)**. It is found that while there is an increase in absorption in the front cell, the back-cell absorption is ceasing in the range of the front cell. The front cell shows a current density of 10.87 mA/cm$^2$, and the

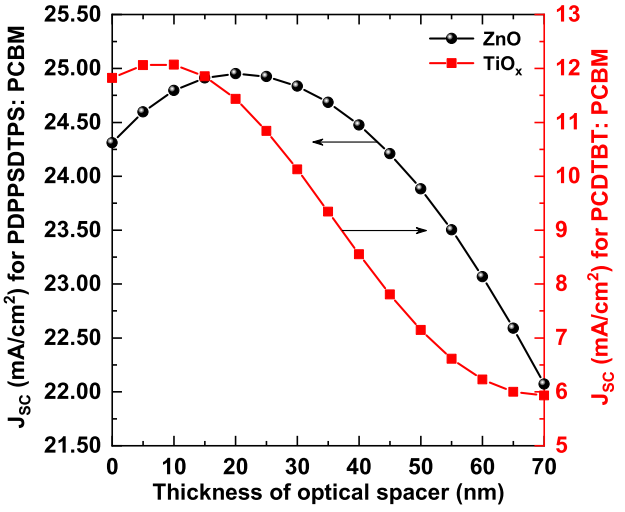


**FIGURE 7.** Short-circuit current density, $J_{SC}$ of various optical spacer thicknesses. $TiO_x$ and ZnO are employed as optical spacer materials for PCDTBT: PCBM and PDPPSDTPS: PCBM, respectively.

back subcell shows 16.9 mA/cm$^2$ at this thickness, assuming 100% IQE. But there is a noticeable current mismatching between the two cells.

### C. TRIPLE-JUNCTION OSC

From the absorption curve of **Fig. 8 (b)**, it can be seen that from 550 to 750 nm, there is inferior absorption of photons, which further opens the door for a middle layer. We have chosen some high-performance organic materials for the middle layer that show considerable absorption in this range to design an efficient triple-junction structure. The device architecture for triple junction is shown in **Fig. 9 (a)**. We have studied the performance of three different triple-junction structures. In all three structures, the front cell and back cell constituents are PCDTBT: PCBM and PMDPP3T: PCBM, respectively, and the middle layer has three different organic materials for each structure. These OSCs are defined as Triple 1, Triple 2, and Triple 3 where the middle cell consists of PTB7:PCBM, PTB7-Th:PCBM, and pBBTDPP2:PCBM, respectively. One of the biggest challenges for multijunction OSC is obtaining a high balanced current density for all the concerned subcells. We have tried different combinations of thicknesses for the active layers to achieve a maximum and matched current from triple-junction structures. After careful optimization of thickness, the maximum and matched current is noted for all the subcells. The absorption profile of the concerned subcells in their respective triple-junction structures with these optimized thicknesses is shown in **Fig. 9 (b)** which shows all three subcells of the triple junction structures display considerable absorption in their respective position. The current density of the individual subcells at the optimized thickness and the percentage of current mismatch are summarized in **TABLE 2**. From the table, it is found that the back-cell thickness is lower for structures 1 and 2, but a larger thickness is required for structure 3. The middle cell in structure 3 has an absorption range up to 900 nm that reduces the amount of photon

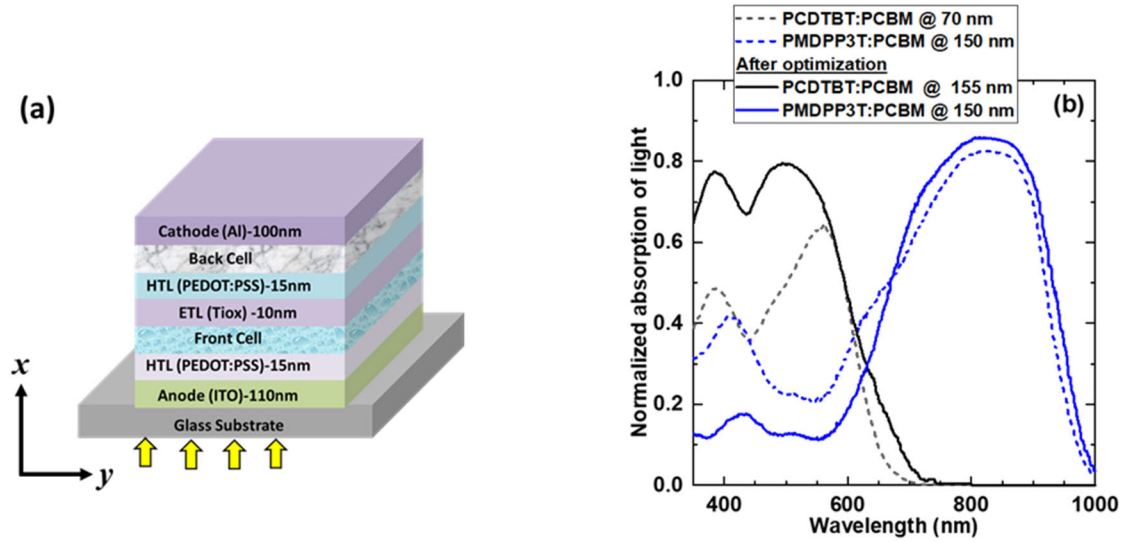


**FIGURE 8.** Device architecture (a) and absorption spectra of PCDTBT:PCBM and PMDPP3T:PCBM (b) for double-junction OSC.

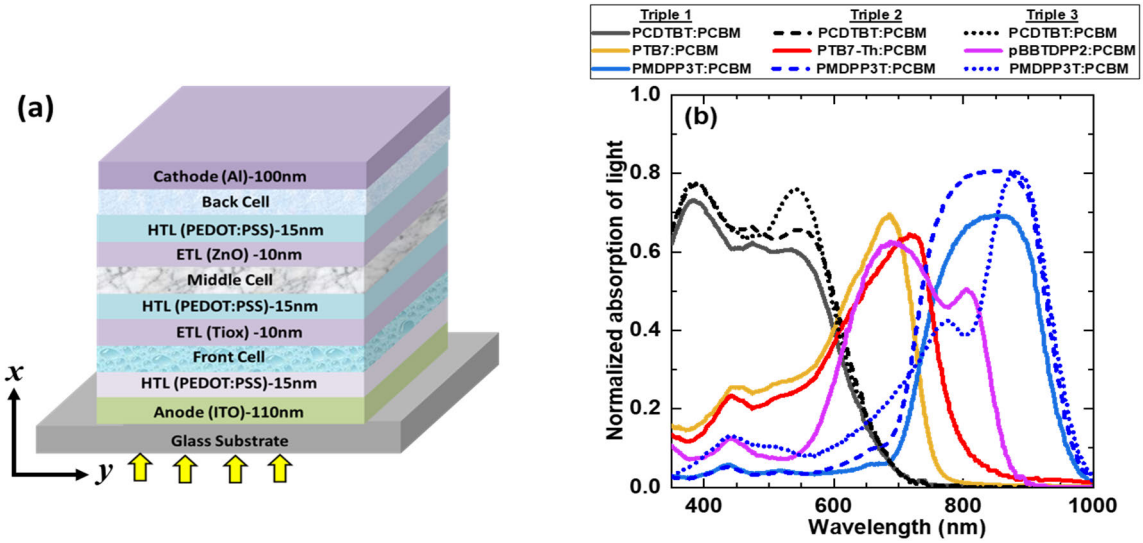


**FIGURE 9.** Device architecture (a) and absorption spectra of individual active layers (b) for the triple-junction of OSC.

**TABLE 2.** Performances of triple junction structures of proposed OSCs.

| Name of OSC | Device Structure | Optimized thickness (nm) | $J_{SC}$ (mA/cm$^2$) | Current mismatch (%) |
|---|---|---|---|---|
| Triple 1 | Front Cell (PCDTBT:PCBM) | 132 | 9.0254 | 0 |
| | Middle Cell (PTB7:PCBM) | 225 | 9.0802 | 0.6 |
| | Back Cell (PMDPP3T:PCBM) | 100 | 9.0293 | 0.04 |
| Triple 2 | Front Cell (PCDTBT:PCBM) | 155 | 9.9627 | 0.2 |
| | Middle Cell (PTB7-Th:PCBM) | 195 | 9.9470 | 0.11 |
| | Back Cell (PMDPP3T:PCBM) | 124 | 9.9351 | 0 |
| Triple 3 | Front Cell (PCDTBT:PCBM) | 155 | 10.2085 | 0 |
| | Middle Cell (pBBTDPP2:PCBM) | 145 | 10.2274 | 0.185 |
| | Back Cell (PMDPP3T:PCBM) | 170 | 10.3556 | 1.44 |

harvested by the back cell. So, a higher thickness is needed for the back cell for considerable absorption in this structure. Again PTB7-Th:PCBM and pBBTDPP2:PCBM have extended absorption than PTB7:PCBM. Therefore, among the middle cells, PTB7:PCBM required higher thickness due to its narrow absorption range. It is found that Triple 3

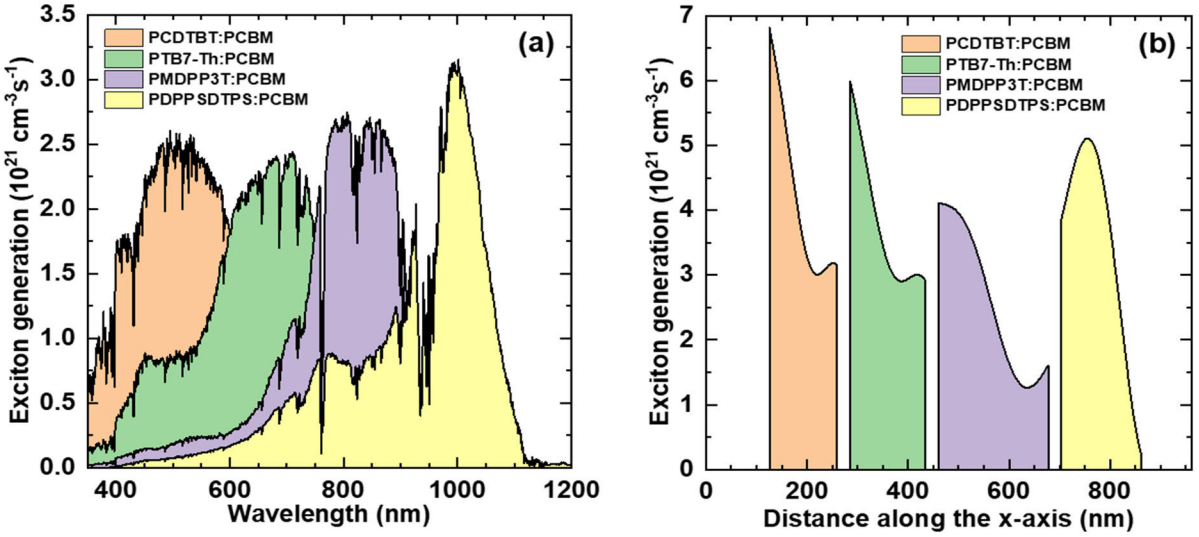


**FIGURE 10.** Exciton generation of individual subcells as a function of wavelength (a) and along the x-axis of quadruple 2 OSC (b).

provides the best current to be achieved than the other two OSCs. The current mismatch is calculated, and the optimized triple-junction cells provide good current matching in all structures.

### D. QUADRUPLE-JUNCTION OSC

The detailed materials and thicknesses of each layer have been shown in **Fig. 1**. The limited performance of organic tandem cells is primarily due to their limited absorption range due to the lack of optimal low-bandgap materials for the back subcell. Thus, a large part of the entire solar spectrum remains unabsorbed. In our proposed triple junction structures, we have seen the maximum absorption is limited to 1000 nm. A low-bandgap material with extended absorption more than this range would open the gate for a next junction to be added. The low bandgap material PDPPSDTPS: PCBM material shows a photo response extending to 1200 nm. The proposed quadruple junction structure absorbs photons from 350 to 1200 nm. The final efficiency of quadruple junction solar cell devices strongly depends on the individual subcells' current matching. We have assured current matching for our proposed quadruple structures while increasing the absorption efficiency by thickness optimization. There are three different quadruple-junction structures are considered where front cell, middle back cell, and back cell consist of fixed PCDTBT: PCBM, PMDPP3T:PCBM, and PDPPSDTPS:PCBM, respectively. While only the middle front cell is altered to construct the OSCs, which define as quadruple 1, quadruple 2, and quadruple 3 with PTB7:PCBM, PTB7-Th: PCBM, and pBBTDPP2:PCBM, respectively. The thickness of all the active layers constituting the quadruple structure is varied simultaneously to find the optimum combination where the current is maximum, and the current mismatch will be minimum. Based on our simulation results, the best short-circuit current density would be achieved from the quadruple 2. **Figure 10** shows the individual contribution to the subcells' exciton generation in quadruple 2 at optimized thickness. It is found from **Fig. 10 (a)** that photons are absorbed by the previous layer of a structure for all subcells except the front subcell. Spectral overlapping by the successive layers causes lowered absorption of individual active layers. If photon absorption is reduced, the current density is found low.

All the constituent layers employ in the structure directly influence the performance of the device. We have studied how changing the thickness of one subcell affects other subcells in our proposed quadruple structures. We have considered the quadruple 2 which shows the highest achievable current among the other quadruple structures. The thickness of individual subcells has been varied while keeping the thicknesses constant at optimized layer thickness for all other layers as shown in **Fig. 11**. It is observed that increasing the thickness of one layer will surely increase that concerned layer's current as higher thickness ensures higher absorption. Changing a layer thickness has succeeding effects on other layers, and current matching is difficult for quadruple junction solar cells. In all cases, when we increase the thickness of one layer, it decreases the subsequent next subcell's current. This phenomenon is realized as the increasing thickness of one layer may leave less photon to harvest in the consequent layer. For the other two subcells, the decrease in current is small and shows almost linear behavior. It can conclude that layers are very much correlated in their multijunction structure from thickness optimization analysis. Changing the thickness of one layer has subsequent effects in their former and next layers. It is also be found that at one point, the entire curve intersects, and the current of all subcells have nearly the same value. This is the match current for the thickness of the respective subcell.

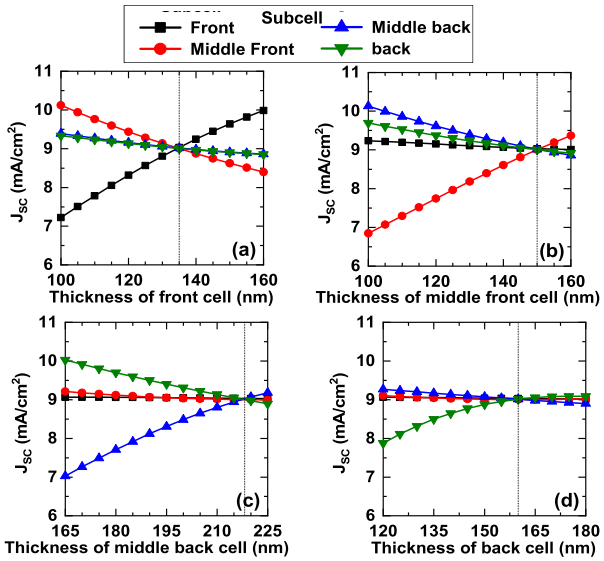


**FIGURE 11.** Active layer thickness-dependent short-circuit current density, $J_{SC}$ for different subcells of quadruple 2.

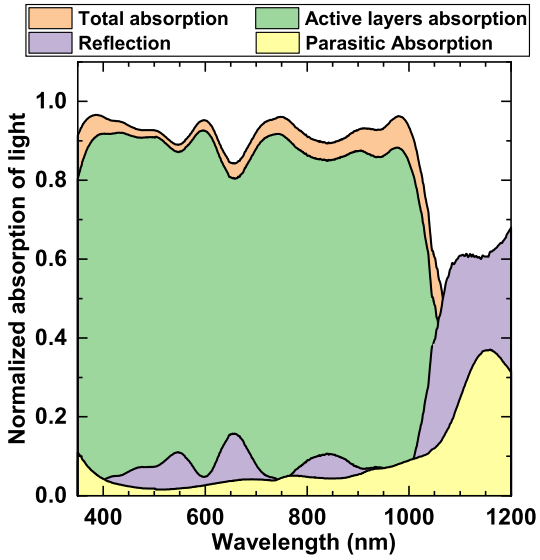


**FIGURE 12.** Total active layer absorption, reflection, and parasitic absorption of quadruple 2.

Parasitic absorption refers to an optical absorption that does not generate an EHP pair. Parasitic absorptions in non-active layers influence the photogenerated carrier profile in OSCs. For the proposed quadruple structures, thirteen layers are employed; four layers are the photoactive layers. **Figure 12** shows that most of the absorption is by the OPV materials in our proposed quadruple 2. As the material chosen for recombination layers and interlayer shows high optical transparency, i.e., low optical absorption in the region of interest, parasitic absorption is not limiting in the proposed quadruple-junction OSC.

The maximum current density has been estimated by thickness optimization for proposed quadruple structures. The thicknesses of the active layers varied from 70 to 220 nm.

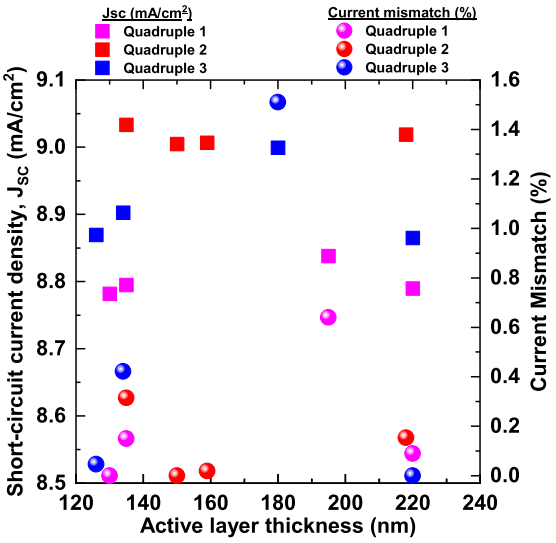


**FIGURE 13.** Short-circuit current density, $J_{SC}$, and current mismatch for different quadruple OSCs.

Increasing the thickness of the active layer can improve short-circuit current density. Simultaneously, a thicker device requires higher mobility of charge carriers to ensure efficient charge collection at their respective electrodes. The current density of the individual subcells at the optimized thickness and the percentage of current mismatch of quadruple structures are summarized in **TABLE 3** and shown in **Fig. 13**. A considerable increase in thickness for middle back cells in all the proposed model structures can be observed (195 nm, 218 nm, and 220 nm). The material used for the middle back cell, i.e., PMDPP3T: PCBM, has electron and hole mobilities in the range of $10^{-2}$– $10^{-3}$ cm$^2$V$^{-1}$s$^{-1}$ [31]. Therefore, this material's mobility is strong enough for efficient charge collection at these thicknesses can be realized. Whenever we have used pBBTDPP2:PCBM as the middle layer in our triple-junction structure, it shows a high maximum achievable current than the other two structures. It works well for its quadruple structure position however reduces the photon absorption of the middle back layer PMDPP3T: PCBM, which is the current limiting subcell. As the middle back layer is sandwiched between pBBTDPP2:PCBM and PDPPSDTPS: PCBM, they leave a narrow absorption range and less photon to harvest for the middle back subcell. From the observation of achievable current density, the proposed quadruple 2 gives the best current density to be achieved than the other two structures.

### *E. COMPARATIVE STUDY OF OSCS*

In a single-junction, we have found better performance for small thicknesses of active layers. However, when these materials are employed as a subcell in tandem, a considerable thickness is required to achieve better current density. An important reason behind the limited tandem cell current is owing to the absorption overlapping. The back electrode will reflect the photons that are not absorbed in the first pass,

**TABLE 3.** Performances of quadruple junction structures of proposed OSCs.

| Name of OSC | Device Structure | Optimized thickness (nm) | $J_{SC}$ (mA/cm$^2$) | Current mismatch (%) |
|---|---|---|---|---|
| Quadruple 1 | Front Cell (PCDTBT:PCBM) | 130 | 8.7816 | 0 |
| | Middle Front Cell (PTB7:PCBM) | 220 | 8.7896 | 0.09 |
| | Middle Back Cell (PMDPP3T:PCBM) | 195 | 8.8378 | 0.64 |
| | Back Cell (PDPPSDTPS:PCBM) | 135 | 8.7947 | 0.15 |
| Quadruple 2 | Front Cell (PCDTBT:PCBM) | 135 | 9.0329 | 0.315 |
| | Middle Front Cell (PTB7-Th:PCBM) | 150 | 9.0045 | 0 |
| | Middle Back Cell (PMDPP3T:PCBM) | 218 | 9.0184 | 0.154 |
| | Back Cell (PDPPSDTPS:PCBM) | 159 | 9.0062 | 0.0189 |
| Quadruple 3 | Front Cell (PCDTBT:PCBM) | 126 | 8.8691 | 0.047 |
| | Middle Front Cell (pBBTDPP2:PCBM) | 134 | 8.9023 | 0.422 |
| | Middle Back Cell (PMDPP3T:PCBM) | 220 | 8.8649 | 0 |
| | Back Cell (PDPPSDTPS:PCBM) | 180 | 8.9991 | 1.51 |

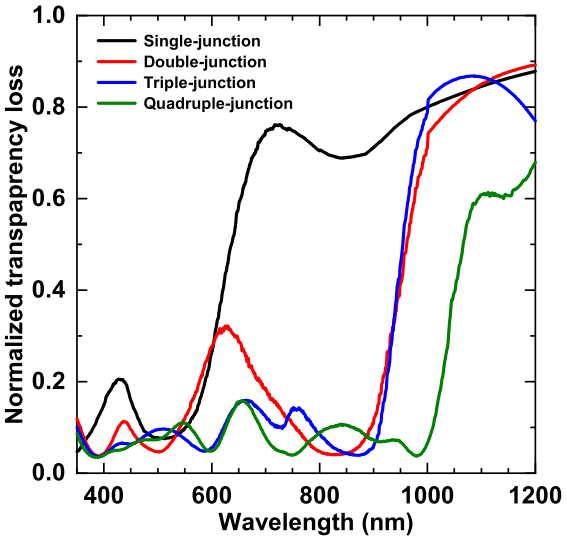


**FIGURE 14.** Normalized transparency loss for different junctions.

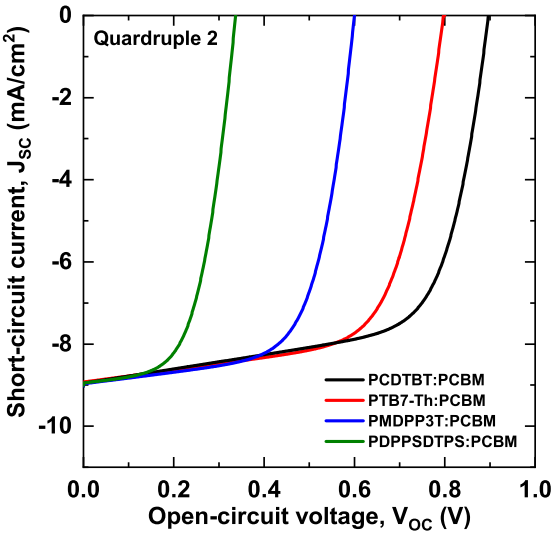


**FIGURE 15.** J-V characteristics curve of concerned subcells in quadruple 2 OSC.

and there is a possibility that these photons can be absorbed in the second pass [24]. For multijunction cells, these photons are usually absorbed by the subsequent layer. Furthermore, complete absorption is impossible with the thickness we have used for our simulation (100 - 225 nm). The reflection loss in OSCs is considered as shown in **Fig. 14**. Incident radiation reflected off from the interfaces of ITO, PEDOT: PSS, etc. In the single-junction where the active material is PCDTBT: PCBM, the reflection losses are rising when the absorption of the active layer is ceasing. In double-junction, the back subcell PMDPP3T: PCBM shows good absorption up to 900 nm. The reflection loss is increased after this range. **Figure 8(b)** shows an absorption window where both subcells of double junction structure cannot show good absorption. This range increase of normalized transparency loss is observed, further minimized by adding middle layer PTB7-Th: PCBM in triple junction. By adding low bandgap material PDPPSDTPS: PCBM in quadruple structure, transparency loss reduced to 1000 nm.

Namkoong *et al.* reported the experimental work that though the variation of photoactive layer thickness has a mentionable impact on the short circuit current density, the open-circuit voltage remains almost constant with varying thickness [20]. The total open-circuit voltage of the series-connected tandem solar cell is equal to the sum of the single-junction cells' voltage. Many experimental works also support this phenomenon. You *et al.* experimentally showed that the open-circuit voltage is ∼0.01V less than that of the front and rear cell voltage combination [2], which may arise from interconnecting layers' small resistances. The value of $V_{OC}$ is calculated for the materials concerning experimental data [26], [29]–[32], [51]. The reported value of fill-factor (FF) of different subcells of the proposed quadruple OSC is usually in the range of 0.65 except for PDPPSDTPS:PCBM (FF = 0.57) [32]. We have considered the losses, so that over-estimation of PCE is avoided. The J-V characteristics of different subcells of the proposed quadruple 2 are shown in **Fig. 15**. Considering all optimized structure and losses, we

**TABLE 4.** Comparison between different Tandem OSCs with our simulated one.

| OSC | Device Architecture | $J_{SC}$ (mA/cm$^2$) | $V_{OC}$ (V) | FF (%) | PCE (%) |
|---|---|---|---|---|---|
| Double Junction | PCDTBT:PCBM (155 nm) /PMDPP3T:PCBM (150 nm) **[31]** | 9.58 | 1.49 | 62 | 8.90 |
| | PCDTBT:PCBM (70 nm)/ PMDPP3T:PCBM (150 nm) **[52]** | 10.38 | 1.48 | 65 | 10.0 |
| | P3HT:PCBM (350 nm)/ PTB7:PCBM (90 nm) **[6]** | 22.60 | 0.85 | 68.21 | 13.96 |
| | PCDTBT:PCBM (155 nm) /PMDPP3T:PCBM (150 nm) **[This work]** | 10.87 | 1.50 | 65 | 10.59 |
| Triple Junction | PCDTBT:PCBM (125 nm)/ PMDPP3T:PCBM (95 nm) /PMDPP3T:PCBM (215 nm) **[31]** | 7.34 | 2.09 | 65 | 9.64 |
| | P3HT:ICBA(160 nm)/PTB:PCBM (110 nm) /LBG:PCBM(85 nm) **[53]** | 7.63 | 2.28 | 66 | 11.55 |
| | PCDTBT:PCBM (155 nm)/PTB7-Th:PCBM (195 nm) /PMDPP3T:PCBM (124 nm) **[This work]** | 9.935 | 2.3 | 65 | 14.85 |
| Quadruple Junction | PDCBT:PCBM (110 nm) /PTB7-Th:PCBM (100 nm) /PMDPP3T:PCBM (170 nm) /PDPPSDTPS:PCBM (160 nm) **[24]** | 5.26 | 2.46 | 63 | 8.2 |
| | PCDTBT:PCBM (135 nm) /PTB7-Th:PCBM (150 nm) /PMDPP3T:PCBM (218 nm) / PDPPSDTPS:PCBM (159 nm) **[This work]** | **9.00** | **2.64** | **65** | **15.45** |

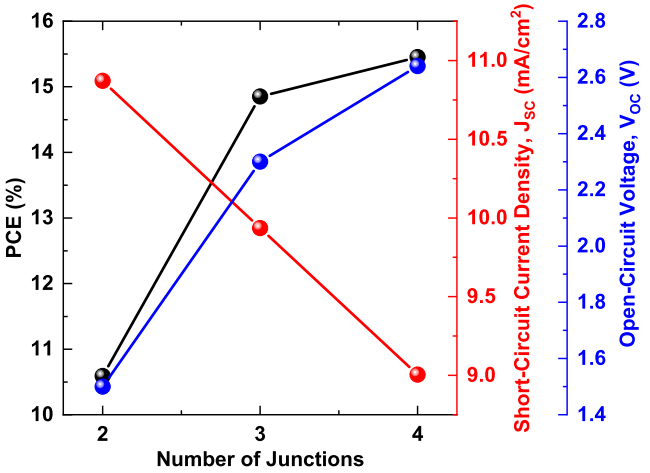


**FIGURE 16.** Variation of short-circuit current density, $J_{SC}$, open-circuit voltage, $V_{OC}$, and power conversion efficiency, PCE for different tandem OSCs.

have calculated the PCE of the proposed double, Triple 2, and Quadruple 2 OSCs. The FF is assumed as 0.65, which is the state-of-the-art value. The overall device performances are shown in **Fig. 16**. The $J_{SC}$ is found to be reduced by adding more junctions. The lowest current is observed for the quadruple 2. Though the $J_{SC}$ is low in quadruple 2, the PCE is expected to be improved because of series-connected junctions. Adding junctions in tandem structure means summing up their individual $V_{OC}$. The comparison of our simulated devices' performance with other reported device architectures is shown in **TABLE 4**. The proposed quadruple OSC (quadruple 2) has a potential to achieve the high PCE of 15.45%. Above studies also suggest that organic materials employed in tandem solar cells are highly promising for high-performance photovoltaic applications.

## IV. CONCLUSION

This paper represents the systematic study of tandem OSCs using optical modeling, and the simulation results give the prediction about their performances. In multijunction OSC, the entire cell's current is determined by the lowest current supplied by any of the subcells. A careful selection of material is essential as the short-circuit current is the efficiency limiting factor. For a fixed thickness, concerned subcells show less current in their tandem structure than single-junction due to the absorption overlapping. In tandem OSC, the individual subcells' structure thicknesses must be optimized, and current density needs to be matched to achieve better photovoltaic characteristics. As organic materials' thickness is limited between a few hundred nanometers, the maximization of current density and matched current of individual subcells is a tough task as more junctions are added. We have proposed double, triple, and quadruple junction OSC with proper consideration of thickness and current matching of different subcells. The maximum current mismatch found in the optimized structures is 1.5% that means the current matching of all subcells in their tandem configuration is ensured. The impact of changing one layer's thickness on other subcells' currents is also discussed. The maximum achievable current density is 9.00 mA/cm$^2$, along with the open-circuit voltage of 2.64 V, found in the proposed optimized quadruple OSC. This OSC also offers a PCE of about 15.45% with FF = 0.65. The PCE increases by ~40% and ~46% compared to triple-junction and double-junction structures, respectively. The

quadruple junction's reduced current is over-compensated by the quadruple structure's back layer's open-circuit voltage. These results indicate that quadruple-junction solar cells are very encouraging for next-generation photovoltaic applications.

## REFERENCES

[1] A. Pivrikas, H. Neugebauer, and N. S. Sariciftci, "Charge carrier lifetime and recombination in bulk heterojunction solar cells," *IEEE J. Sel. Topics Quantum Electron.*, vol. 16, no. 6, pp. 1746–1758, Dec. 2010, doi: 10.1109/JSTQE.2010.2044978.

[2] J. You, L. Dou, K. Yoshimura, T. Kato, K. Ohya, T. Moriarty, K. Emery, C.-C. Chen, J. Gao, G. Li, and Y. Yang, "A polymer tandem solar cell with 10.6% power conversion efficiency," *Nature Commun.*, vol. 4, no. 1, p. 1446, Feb. 2013, doi: 10.1038/ncomms2411.

[3] J. Hou, O. Inganäs, R. H. Friend, and F. Gao, "Organic solar cells based on non-fullerene acceptors," *Nature Mater.*, vol. 17, no. 2, pp. 119–128, Jan. 2018, doi: 10.1038/nmat5063.

[4] Z. Xiao, X. Jia, and L. Ding, "Ternary organic solar cells offer 14% power conversion efficiency," *Sci. Bull.*, vol. 62, no. 23, pp. 1562–1564, Dec. 2017, doi: 10.1016/j.scib.2017.11.003.

[5] Y. Liang, Z. Xu, J. Xia, S.-T. Tsai, Y. Wu, G. Li, C. Ray, and L. Yu, "For the bright future-bulk heterojunction polymer solar cells with power conversion efficiency of 7.4%," *Adv. Mater.*, vol. 22, no. 20, pp. E135–E138, May 2010, doi: 10.1002/adma.200903528.

[6] W. Farooq, A. D. Khan, A. D. Khan, A. Rauf, S. D. Khan, H. Ali, J. Iqbal, R. U. Khan, and M. Noman, "Thin-film tandem organic solar cells with improved efficiency," *IEEE Access*, vol. 8, pp. 74093–74100, 2020, doi: 10.1109/ACCESS.2020.2988325.

[7] N. Karim, F. I. Mime, M. R. Islam, and I. M. Mehedi, "Tandem organic solar cells with improved efficiency," in *Proc. Int. Conf. Electr., Comput. Commun. Eng. (ECCE)*, Cox's Bazar, Bangladesh, Feb. 2017, pp. 820–825, doi: 10.1109/ECACE.2017.7913016.

[8] T. Ameri, N. Lia, and C. J. Brabec, "Highly efficient organic tandem solar cells: A follow up review," *Energy Environ. Sci.*, vol. 6, no. 8, pp. 2390–2413, May 2013, doi: 10.1039/C3EE40388B.

[9] S. M. Arnab and M. Z. Kabir, "An analytical model for analyzing the current-voltage characteristics of bulk heterojunction organic solar cells," *J. Appl. Phys.*, vol. 115, no. 3, Jan. 2014, Art. no. 034504, doi: 10.1063/1.4861725.

[10] M. Saleheen, S. Arnab, and M. Kabir, "Analytical model for voltage-dependent photo and dark currents in bulk heterojunction organic solar cells," *Energies*, vol. 9, no. 6, p. 412, May 2016, doi: 10.3390/en9060412.

[11] M. S. Islam, "Analytical modeling of organic solar cells including monomolecular recombination and carrier generation calculated by optical transfer matrix method," *Organic Electron.*, vol. 41, pp. 143–156, Feb. 2017, doi: 10.1016/j.orgel.2016.10.040.

[12] L. A. A. Pettersson, L. S. Roman, and O. Inganäs, "Modeling photocurrent action spectra of photovoltaic devices based on organic thin films," *J. Appl. Phys.*, vol. 86, no. 1, pp. 487–496, Jul. 1999, doi: 10.1063/1.370757.

[13] F. Monestier, J.-J. Simon, P. Torchio, L. Escoubas, F. Flory, S. Bailly, R. de Bettignies, S. Guillerez, and C. Defranoux, "Modeling the short-circuit current density of polymer solar cells based on P3HT: PCBM blend," *Sol. Energy Mater. Sol. Cells*, vol. 91, no. 5, pp. 405–410, Mar. 2007, doi: 10.1016/j.solmat.2006.10.019.

[14] M. M. Chowdhury and M. K. Alam, "An optoelectronic analytical model for bulk heterojunction organic solar cells incorporating position and wavelength dependent carrier generation," *Sol. Energy Mater. Sol. Cells*, vol. 132, pp. 107–117, Jan. 2015, doi: 10.1016/j.solmat.2014.08.038.

[15] M. M. Chowdhury and M. K. Alam, "An analytical model for bulk heterojunction organic solar cells using a new empirical expression of space dependent photocarrier generation," *Sol. Energy*, vol. 126, pp. 64–72, Mar. 2016, doi: 10.1016/j.solener.2015.12.050.

[16] L. Liu and G. Li, "Investigation of recombination loss in organic solar cells by simulating intensity-dependent current–voltage measurements," *Sol. Energy Mater. Sol. Cells*, vol. 95, no. 9, pp. 2557–2563, Sep. 2011, doi: 10.1016/j.solmat.2011.02.034.

[17] V. D. Mihailetchi, L. J. A. Koster, J. C. Hummelen, and P. W. M. Blom, "Photocurrent generation in polymer-fullerene bulk heterojunctions," *Phys. Rev. Lett.*, vol. 93, no. 21, Nov. 2004, Art. no. 216601, doi: 10.1103/PhysRevLett.93.216601.

[18] L. Onsager, "Initial recombination of ions," *Phys. Rev.*, vol. 54, no. 8, pp. 554–557, Oct. 1938, doi: 10.1103/PhysRev.54.554.

[19] A. H. Fallahpour, A. Gagliardi, F. Santoni, D. Gentilini, A. Zampetti, M. Auf der Maur, and A. Di Carlo, "Modeling and simulation of energetically disordered organic solar cells," *J. Appl. Phys.*, vol. 116, no. 18, Nov. 2014, Art. no. 184502, doi: 10.1063/1.4901065.

[20] G. Namkoong, J. Kong, M. Samson, I.-W. Hwang, and K. Lee, "Active layer thickness effect on the recombination process of PCDTBT: $PC_{71}BM$ organic solar cells," *Organic Electron.*, vol. 14, no. 1, pp. 74–79, Jan. 2013, doi: 10.1016/j.orgel.2012.10.025.

[21] M. S. S. Rahman and M. K. Alam, "Effect of angle of incidence on the performance of bulk heterojunction organic solar cells: A unified optoelectronic analytical framework," *AIP Adv.*, vol. 7, no. 6, Jun. 2017, Art. no. 065101, doi: 10.1063/1.4985049.

[22] P. Peumans, A. Yakimov, and S. R. Forrest, "Small molecular weight organic thin-film photodetectors and solar cells," *J. Appl. Phys.*, vol. 93, no. 7, pp. 3693–3723, Apr. 2003, doi: 10.1063/1.1534621.

[23] S. Altazin, R. Clerc, R. Gwoziecki, G. Pananakakis, G. Ghibaudo, and C. Serbutoviez, "Analytical modeling of organic solar cells and photodiodes," *Appl. Phys. Lett.*, vol. 99, pp. 143301-1–143301-3, Oct. 2011, doi: 10.1063/1.3643126.

[24] D. Di Carlo Rasi, K. H. Hendriks, M. M. Wienk, and R. A. J. Janssen, "Quadruple junction polymer solar cells with four complementary absorber layers," *Adv. Mater.*, vol. 30, no. 40, Oct. 2018, Art. no. 1803836, doi: 10.1002/adma.201803836.

[25] O. Adebanjo, B. Vaagensmith, and Q. Qiao, "Double junction polymer solar cells," *J. Mater. Chem. A*, vol. 2, no. 27, pp. 10331–10349, 2014, doi: 10.1039/C4TA00470A.

[26] S. H. Park, A. Roy, S. Beaupré, S. Cho, N. Coates, J. S. Moon, D. Moses, M. Leclerc, K. Lee, and A. J. Heeger, "Bulk heterojunction solar cells with internal quantum efficiency approaching 100%," *Nature Photon.*, vol. 3, no. 5, pp. 297–302, Apr. 2009, doi: 10.1038/nphoton.2009.69.

[27] A. Guerrero, N. F. Montcada, J. Ajuria, I. Etxebarria, R. Pacios, G. Garcia-Belmonte, and E. Palomares, "Charge carrier transport and contact selectivity limit the operation of PTB7-based organic solar cells of varying active layer thickness," *J. Mater. Chem. A*, vol. 1, no. 39, pp. 12345–12354, Aug. 2013, doi: 10.1039/C3TA12358H.

[28] L. Huang, X. Cheng, J. Yang, L. Zhang, W. Zhou, S. Xiao, L. Tan, L. Chen, and Y. Chen, "High-performance polymer solar cells realized by regulating the surface properties of PEDOT: PSS interlayer from ionic liquids," *ACS Appl. Mater. Interfaces*, vol. 8, no. 40, pp. 27018–27025, Oct. 2016, doi: 10.1021/acsami.6b09078.

[29] M. M. Wienk, M. Turbiez, J. Gilot, and R. A. J. Janssen, "Narrow-bandgap diketo-pyrrolo-pyrrole polymer solar cells: The effect of processing on the performance," *Adv. Mater.*, vol. 20, no. 13, pp. 2556–2560, Jul. 2008, doi: 10.1002/adma.200800456.

[30] O. Amargós-Reyes, J.-L. Maldonado, D. Romero-Borja, D. Barreiro-Argüelles, I. Caballero-Quintana, O. Barbosa-García, and J. A. Gaspar, "Organic photovoltaic cell analysis through quantum efficiency and scanning tunneling microscopy of the donor/blend as an active film," *J. Mater. Sci.*, vol. 54, no. 3, pp. 2427–2445, Sep. 2018, doi: 10.1007/s10853-018-2956-2.

[31] W. Li, A. Furlan, K. H. Hendriks, M. M. Wienk, and R. A. J. Janssen, "Efficient tandem and triple-junction polymer solar cells," *J. Amer. Chem. Soc.*, vol. 135, no. 15, pp. 5529–5532, Apr. 2013, doi: 10.1021/ja401434x.

[32] K. H. Hendriks, W. Li, M. M. Wienk, and R. A. J. Janssen, "Small-bandgap semiconducting polymers with high near-infrared photoresponse," *J. Amer. Chem. Soc.*, vol. 136, no. 34, pp. 12130–12136, Aug. 2014, doi: 10.1021/ja506265h.

[33] M. Rumbak, I. Visoly-Fisher, and R. Shikler, "Broadband absorption enhancement via light trapping in periodically patterned polymeric solar cells," *J. Appl. Phys.*, vol. 114, no. 1, Jul. 2013, Art. no. 013102, doi: 10.1063/1.4812324.

[34] A. Armin, M. Velusamy, P. Wolfer, Y. Zhang, P. L. Burn, P. Meredith, and A. Pivrikas, "Quantum efficiency of organic solar cells: Electro-optical cavity considerations," *ACS Photon.*, vol. 1, no. 3, pp. 173–181, Feb. 2014, doi: 10.1021/ph400044k.

[35] C. Stelling, C. R. Singh, M. Karg, T. A. F. König, M. Thelakkat, and M. Retsch, "Plasmonic nanomeshes: Their ambivalent role as transparent electrodes in organic solar cells," *Sci. Rep.*, vol. 7, no. 1, p. 42530, Feb. 2017, doi: 10.1038/srep42530.

[36] T. Jiang, J. Yang, Y. Tao, C. Fan, L. Xue, Z. Zhang, H. Li, Y. Li, and W. Huang, "Random terpolymer with a cost-effective monomer and comparable efficiency to PTB7-Th for bulk-heterojunction polymer solar cells," *Polym. Chem.*, vol. 7, no. 4, pp. 926–932, 2016, doi: 10.1039/C5PY01771H.

[37] G. Li, V. Shrotriya, Y. Yao, and Y. Yang, "Investigation of annealing effects and film thickness dependence of polymer solar cells based on poly(3-hexylthiophene)," *J. Appl. Phys.*, vol. 98, no. 4, Aug. 2005, Art. no. 043704, doi: 10.1063/1.2008386.

[38] G. F. Burkhard, E. T. Hoke, and M. D. McGehee, "Accounting for interference, scattering, and electrode absorption to make accurate internal quantum efficiency measurements in organic and other thin solar cells," *Adv. Mater.*, vol. 22, no. 30, pp. 3293–3297, Aug. 2010, doi: 10.1002/adma.201000883.

[39] O. Adebanjo, P. P. Maharjan, P. Adhikary, M. Wang, S. Yang, and Q. Qiao, "Triple junction polymer solar cells," *Energy Environ. Sci.*, vol. 6, no. 11, pp. 3150–3170, Aug. 2013, doi: 10.1039/C3EE42257G.

[40] M. C. Scharber, D. Mühlbacher, M. Koppe, P. Denk, C. Waldauf, A. J. Heeger, and C. J. Brabec, "Design rules for donors in bulk-heterojunction solar cells—Towards 10% energy-conversion efficiency," *Adv. Mater.*, vol. 18, no. 6, pp. 789–794, Mar. 2006, doi: 10.1002/adma.200501717.

[41] B. Qi and J. Wang, "Open-circuit voltage in organic solar cells," *J. Mater. Chem.*, vol. 22, no. 46, pp. 24315–24325, Sep. 2012, doi: 10.1039/C2JM33719C.

[42] R. Häusermann, E. Knapp, M. Moos, N. A. Reinke, T. Flatz, and B. Ruhstaller, "Coupled optoelectronic simulation of organic bulk-heterojunction solar cells: Parameter extraction and sensitivity analysis," *J. Appl. Phys.*, vol. 106, no. 10, Nov. 2009, Art. no. 104507, doi: 10.1063/1.3259367.

[43] L. J. A. Koster, E. C. P. Smits, V. D. Mihailetchi, and P. W. M. Blom, "Device model for the operation of polymer/fullerene bulk heterojunction solar cells," *Phys. Rev. B, Condens. Matter*, vol. 72, no. 8, Aug. 2005, Art. no. 085205, doi: 10.1103/PhysRevB.72.085205.

[44] C.-H. Chou, W. L. Kwan, Z. Hong, L.-M. Chen, and Y. Yang, "A metal-oxide interconnection layer for polymer tandem solar cells with an inverted architecture," *Adv. Mater.*, vol. 23, no. 10, pp. 1282–1286, Mar. 2011, doi: 10.1002/adma.201001033.

[45] P. P. Boix, G. Garcia-Belmonte, U. Muñecas, M. Neophytou, C. Waldauf, and R. Pacios, "Determination of gap defect states in organic bulk heterojunction solar cells from capacitance measurements," *Appl. Phys. Lett.*, vol. 95, no. 23, Dec. 2009, Art. no. 233302, doi: 10.1063/1.3270105.

[46] C.-W. Liang, W.-F. Su, and L. Wang, "Enhancing the photocurrent in poly(3-hexylthiophene)/[6,6]-phenyl $C_{61}$ butyric acid methyl ester bulk heterojunction solar cells by using poly(3-hexylthiophene) as a buffer layer," *Appl. Phys. Lett.*, vol. 95, no. 13, Sep. 2009, Art. no. 133303, doi: 10.1063/1.3242006.

[47] Y. Sun, C. J. Takacs, S. R. Cowan, J. H. Seo, X. Gong, A. Roy, and A. J. Heeger, "Efficient, air-stable bulk heterojunction polymer solar cells using MoOx as the anode interfacial layer," *Adv. Mater.*, vol. 23, no. 19, pp. 2226–2230, Apr. 2011, doi: 10.1002/adma.201100038.

[48] J. Y. Kim, S. H. Kim, H.-H. Lee, K. Lee, W. Ma, X. Gong, and A. J. Heeger, "New architecture for high-efficiency polymer photovoltaic cells using solution-based titanium oxide as an optical spacer," *Adv. Mater.*, vol. 18, no. 5, pp. 572–576, Mar. 2006, doi: 10.1002/adma.200501825.

[49] A. Roy, S. H. Park, S. Cowan, M. H. Tong, S. Cho, K. Lee, and A. J. Heeger, "Titanium suboxide as an optical spacer in polymer solar cells," *Appl. Phys. Lett.*, vol. 95, no. 1, Jul. 2009, Art. no. 013302, doi: 10.1063/1.3159622.

[50] M. Islam, S. Wahid, M. M. Chowdhury, F. Hakim, and M. K. Alam, "Effect of spatial distribution of generation rate on bulk heterojunction organic solar cell performance: A novel semi-analytical approach," *Organic Electron.*, vol. 46, pp. 226–241, Jul. 2017, doi: 10.1016/j.orgel.2017.04.021.

[51] H. Aqoma, S. Park, H.-Y. Park, W. T. Hadmojo, S.-H. Oh, S. Nho, D. H. Kim, J. Seo, S. Park, D. Y. Ryu, S. Cho, and S.-Y. Jang, "11% organic photovoltaic devices based on PTB7-Th: $PC_{71}$ BM photoactive layers and irradiation-assisted ZnO electron transport layers," *Adv. Sci.*, vol. 5, no. 7, Jul. 2018, Art. no. 1700858, doi: 10.1002/advs.201700858.

[52] F. I. Mime, M. S. H. Khan, S. M. Asaduzzaman, N. Karim, and M. R. Islam, "Efficient triple junction organic solar cell," in *Proc. IEEE Region Symp. (TENSYMP)*, Dhaka, Bangladesh, Jun. 2020, pp. 198–201, doi: 10.1109/TENSYMP50017.2020.9230594.

[53] C.-C. Chen, W.-H. Chang, K. Yoshimura, K. Ohya, J. You, J. Gao, Z. Hong, and Y. Yang, "An efficient triple-junction polymer solar cell having a power conversion efficiency exceeding 11%," *Adv. Mater.*, vol. 26, no. 32, pp. 5670–5677, Jul. 2014, doi: 10.1002/adma.201402072.

**FARHA ISLAM MIME** received the B.Sc. Engineering degree in electrical and electronic engineering (EEE) from the Khulna University of Engineering and Technology (KUET), in 2016, where she is currently pursuing the M.Sc. Engineering degree in EEE. She is also serving as a Lecturer with the University of Information Technology and Sciences (UITS), Dhaka, Bangladesh. She has published her research papers in national and international conferences. Her research interests include organic photovoltaic cells and organic tandem cell design.

**MD. RAFIQUL ISLAM** (Member, IEEE) received the B.Sc. Engineering degree from the Bangladesh University of Engineering and Technology (BUET), Dhaka, Bangladesh, in 1998, the M.Sc. Engineering degree from the Khulna University of Engineering and Technology (KUET), Khulna, Bangladesh, in 2006, both in electrical and electronic engineering, and the Ph.D. degree in semiconductor device growth, characterization and fabrication from the University of Fukui, Japan, in 2010.

He is currently working as a Professor with the Khulna University of Engineering and Technology. He received the Monbukagakusho scholarship from Japan (MEXT) for the term 2007–2010. He has published around 100 research papers in national and international conferences and journals. His research interests include thin films solar cells, growth characterization and fabrications, advanced semiconductor materials properties, compound semiconductor-based devices, and so on. His two papers received the Best Paper Award from international conferences.

**EKLAS HOSSAIN** (Senior Member, IEEE) received the B.S. degree in electrical and electronic engineering from the Khulna University of Engineering and Technology, Bangladesh, in 2006, the M.S. degree in mechatronics and robotics engineering from the International Islamic University Malaysia, Malaysia, in 2010, and the Ph.D. degree from the College of Engineering and Applied Science, University of Wisconsin–Milwaukee (UWM). Since 2015, he has been involving with several research projects on renewable energy and grid tied microgrid system at Oregon Tech, as an Assistant Professor with the Department of Electrical Engineering and Renewable Energy. He is currently working as an Associate Researcher with the Oregon Renewable Energy Center (OREC). He is a registered Professional Engineer (PE) in Oregon, USA. He is also a Certified Energy Manager (CEM) and a Renewable Energy Professional (REP). For last ten years, he was worked in the area of distributed power systems and renewable energy integration and has published a number of research papers and posters in this field. His research interests include modeling, analysis, design, and control of power electronic devices, energy storage systems, renewable energy sources, integration of distributed generation systems, microgrid and smart grid applications, robotics, and advanced control systems. With his dedicated research team, he is looking forward to exploring methods to make the electric power systems more sustainable, cost-effective, and secure through extensive research and analysis on energy storage, microgrid systems, and renewable energy sources. He is a Senior Member of the Association of Energy Engineers (AEE). He is a Winner of the Rising Faculty Scholar Award, from the Oregon Institute of Technology, in 2019, for his outstanding contribution in teaching. He currently serves as an Associate Editor for IEEE Access.

**IBRAHIM M. MEHEDI** received the B.Sc. degree (Hons.) in electrical and electronic engineering from the Rajshahi University of Engineering and Technology (RUET), Bangladesh, in 2000, and the M.Sc. degree in aerospace engineering from University Putra Malaysia (UPM), Malaysia, in 2005, and the Ph.D. degree in electrical engineering and information systems from The University of Tokyo, Tokyo, Japan, in 2011. After his B.Sc. degree, he worked with the Coca-Cola Bottling Plant for two years. He was the Principal Investigator in large research and development projects funded by KACST, MOE, and KAU. In 2006, he was appointed as a Lecturer with the King Fahd University of Petroleum and Minerals (KFUPM). From 2008 to 2012, he worked as a Research Assistant and a Postdoctoral Fellow with the Japan Aerospace Exploration Agency (JAXA), Japan. In 2012, he joined the Department of Electrical and Computer Engineering (ECE), King Abdulaziz University (KAU), where he is currently an Associate Professor. He is also a Senior Scientist with the Center of Excellence in Intelligent Engineering Systems (CEIES), King Abdulaziz University. He has been involved in several research and development projects. He has published several journals and conference papers and supervised and co-supervised several M.Sc. and Ph.D. students. His field of interests and specializations include a broad spectrum from theoretical to practical aspects of engineering, including intelligent systems, control, electronic devices, sensors, energy, and artificial intelligence.

**MD. TANVIR HASAN** (Member, IEEE) received the B.Sc. and M.Sc. degrees from the Khulna University of Engineering and Technology (KUET), Bangladesh, in 2006 and 2007, respectively, and the Ph.D. degree from the Graduate School of Engineering, University of Fukui, Japan, in 2013, all in electrical and electronic engineering.

He received the Monbukagakusho scholarship from Japan (MEXT) for the term 2010–2013. He served as a Secretary for being IEEE Young Professional, Bangladesh Section (BDS), and an Executive Committee Member as a Professional Activity Coordinator, IEEE BDS, in 2016 and 2017, respectively. He is currently working as an Associate Professor with the Department of Electrical and Electronic Engineering, Jashore University of Science and Technology (JUST), Bangladesh. He has authored or coauthored more than 50 research papers in conferences and journals. His research interests include growth, design, fabrication, characterization, simulation, and modeling of III-V based semiconductor devices (electronic and optoelectronic). Since 2008, he has been a member of the IEEE Electron Devices Society. He received the IEEE Student Paper Award (Honorary Mentioned) from the IEEE Electron Devices Society, Bangladesh Chapter, in 2007. He serves as a Reviewer for IEEE TRANSACTIONS ON ELECTRON DEVICES, *Journal of Applied Physics*, and *Applied Physics Letters*.